Comparison of Cloud-Type Properties and Radiative Effect Decomposition in Tropical Convectively Active Regions Using CERES High-Resolution Data

Kuan-Man Xu[1], Moguo Sun[2] and Yaping Zhou[3]

1. NASA Langley Research Center, Hampton, VA
2. Analytical Mechanics Associates, Inc./NASA Langley Research Center, Hampton, VA
3. University of Maryland, Baltimore County

Submitted to
Journal of Geophysical Research, Atmosphere

Corresponding author address:
Dr. Kuan-Man Xu
Climate Science Branch
NASA Langley Research Center
Hampton, VA 23681
Email: Kuan-Man.Xu@nasa.gov

Abstract

Land and oceanic convection exhibit significant contrasts in intensity and entrainment, but their effects on the properties of other cloud types remain unclear. This study examines a 19-year mean of cloud properties and top-of-the-atmosphere (TOA) cloud radiative effects (CREs) by cloud type, with a focus on regional variations across convectively active tropical regions. Forty-two cloud types are classified based on effective cloud-top pressure and cloud optical depth. The analysis reveals distinct regional differences in cloud occurrence and properties, with oceanic regions dominated by convective anvils and boundary-layer clouds, which have higher water contents, while land regions feature higher fractions of mid-level clouds with lower liquid water contents. The study further explores shortwave (SW), longwave (LW) and net CREs, decomposing the contributions of individual cloud types to overall CRE differences from tropical means into three components: CRE deviations within a cloud type, cloud fraction (CF) deviations, and their combined effect. Results show that CF deviations have the largest impact, enhancing LW warming and SW cooling for mid- and high-level clouds while reducing SW and net cooling for low-level clouds. Although the effects of CRE deviations are smaller than those of CF deviations for individual cloud types, its collective contribution to overall regional CRE differences, particularly for net CRE, is more comparable, because the former exhibits consistent regional differences across all cloud types while the latter is influenced by opposing effects between low- and high-level clouds. The decomposition analysis also highlights significant regional variations driven by land-ocean contrasts and meteorological forcings.

Key points:

1. This study decomposes regional cloud radiative effect (CRE) differences into three components to assess each cloud type's contribution
2. The cloud fraction (CF) deviation component contributes more to regional CRE differences than the CRE deviation within each cloud type
3. Regional CRE differences from CRE deviation for all cloud types combined are similar to those from CF deviation, especially for net CRE

Plain language summary

This study examines how clouds and their effects on Earth's radiation differ between tropical ocean and land areas. Using 19 years of data, the researchers explore how clouds behave in stormy regions and how each cloud type affects the planet's radiation. They categorized clouds into 42 types based on their height and optical thickness. This study found that ocean areas mostly have more clouds in the lower and upper portions of the atmosphere that hold more water, while land areas have more mid-level clouds with less water. The study also investigates how changes in cloud amounts and types affect regional differences in cloud radiative effects (CRE). It shows that cloud cover amount is the biggest factor in these differences, enhancing the infrared warming and solar cooling effects of high clouds, while reducing the solar cooling effects of low clouds. Even though the effects of CRE changes for a specific cloud type are smaller than those of cloud amount changes, they still matter when effects are summed across all cloud types, especially for net cloud cooling effect. The study concludes that land-ocean differences, along with local weather conditions, are important in shaping cloud patterns and their effects on radiation.

1. Introduction

Clouds play a critical role in regulating the Earth's energy balance through their radiative effects (CREs), which influence the global radiation budget (e.g., Ramanathan et al., 1989; Wielicki et al., 1995, 1996). In the Tropics, regions of intense convection, such as the intertropical convergence zones (ITCZs), are central to energy export to midlatitudes via the Hadley circulation. These areas are often associated with severe weather systems, such as tropical cyclones and mesoscale convective systems (e.g., Mapes, 1993). While deep convective clouds, or "hot towers," are a significant source of latent heat release (Pilewskie et al., 2024; Riehl & Malkus, 1958; Riehl & Simpson, 1979) and drive the Hadley circulation, they occupy only a small portion of the convective system. In fact, the radiative effects of these systems are often dominated by other cloud types, such as expansive convective anvils and low-level clouds (e.g., Feng et al., 2011).

The properties and radiative interactions of clouds—including deep convective clouds—vary considerably across tropical regions (e.g., Kubar et al., 2007; Lin et al., 2010; Yuan et al., 2008). These variations are influenced by factors such as surface type (land vs. ocean), sea surface temperature (SST), atmospheric moisture, aerosols, and dynamic processes. Obviously, regional differences in cloud characteristics are closely linked to the intensity of convective activity, resulting in varying magnitudes of CREs across different cloud types. Understanding these regional differences in cloud properties and their associated CREs is essential for improving climate predictions and addressing uncertainties in cloud feedback (e.g., Luo et al., 2023; Randall et al., 2007; Stephens, 2005; Vial et al., 2013).

It is well-established that convection is generally more intense over land than over ocean, with land convection having broader cores that are less affected by entrainment (e.g., LeMone & Zipser, 1980; Lucas et al., 1994; Takahashi et al., 2023; Xu & Randall, 2001). This difference is

due to the deeper boundary layer over land, which allows larger eddies to be lifted into the free atmosphere, forming broader convective cores. These broader cores are better shielded from the dilution by entrainment, leading to stronger updrafts (e.g., Takahashi et al., 2023). Warmer surface temperatures over land also generate more convective available potential energy (CAPE), although moisture availability over the ocean can moderate land-ocean contrasts. However, moisture has greater effect on other cloud types, particularly low-level clouds, in ways that that may be more significant than its impact on deep convective clouds, as these clouds are less influenced by CAPE. Despite these known differences in convective intensity, entrainment and environmental conditions including aerosols, it remains unclear how these factors influence the regional differences in properties and radiative effects of other cloud types.

To better understand the regional differences in CRE, this study relates them to variations in cloud properties and the environmental conditions that shape different cloud types. Bony et al. (2004) proposed a method to decompose CREs using large-scale pressure vertical velocity at 500 hPa (ω) to separate the dynamic and thermodynamic components of cloud changes in the Tropics. This dynamic regime decomposition isolated changes in CRE resulting from alterations in the large-scale atmospheric circulation from changes in CRE within a regime. This approach has been useful to understand cloud feedback, particularly for low-level clouds (Bony & Dufresne, 2005; Vial et al., 2013). Xu & Cheng (2016) extended this approach to include joint dynamic and stability regimes. In this study, we propose a method to decompose CRE difference between two regions into three components for individual cloud types: CRE deviations within a cloud type (analogous to the thermodynamic component), cloud fraction deviations (analogous to the dynamic component) and their combined effects. An advantage of this approach is that it directly uses cloud types instead of relying on proxies. In previous methods, the subsidence (stable) regime was used

as a proxy for low-level clouds, while the ascending (unstable) regime was associated with deep convective clouds. Weakly ascending or descending (nearly neutral) regimes encompassed a mix of cloud types. It is important to note that cloud types have been defined differently in previous studies, depending on the datasets used (e.g., Burleyson et al., 2015; Hang et al., 2019; Hartmann et al., 1992; Hill et al., 2018; L'Ecuyar et al., 2019; Luo et al., 2023; Najarian & Sakaeda, 2023; Ockert-Bell & Hartmann, 1992; Zhao, 2024).

This study uses the Clouds and the Earth's Radiant Energy System (CERES; Wielicki et al., 1996) FluxByCldTyp (FBCT) dataset (Sun et al., 2022), which provides daily, global, gridded observations of cloud properties and radiative fluxes according to cloud type. The dataset includes 42 distinct cloud types, categorized by effective cloud-top pressure and cloud optical depth. We focus on five tropical regions—the Tropical Western Pacific (TWP), East Pacific and Atlantic ITCZs, equatorial Africa, and the Amazon—collectively known as the "chimney zones" due to their high convective activity (Pilewskie et al., 2024; Riehl & Malkus, 1958; Riehl & Simpson, 1979; Takahashi et al., 2017; William & Stanfill, 2002). These regions represent diverse tropical environments with varying surfaces, atmospheric stability, moisture availability, aerosols, and dynamic processes, leading to significant differences in the frequency of occurrence ("cloud fraction") and properties of cloud types and associated radiative effects.

The primary aim of this study is to compare regional cloud fraction and properties and CREs across these five chimney regions, as well as tropical ocean and land areas. We further analyze how individual cloud types contribute to overall CRE differences from the tropical mean using the decomposition method for assessing the relative importance of deviations in CRE within a cloud type and those in cloud fraction (CF). By doing so, we aim to provide a more detailed understanding of regional variations in CREs and their relationships to cloud properties and

environmental conditions. The findings will enhance our understanding of how regional cloud characteristics contribute to the Earth's radiative balance (e.g., Ceppi & Nowack, 2021; Kubar et al., 2007; Ockert-Bell & Hartmann, 1992; Yuan et al., 2008), with important implications for both regional and global climate modeling.

The rest of this paper is organized as follows: Section 2 describes the FBCT dataset and the CRE decomposition method; Section 3 presents the results; and Section 4 provides summary and discussion.

2. Dataset and methodology

2.1 FluxByCldTyp (FBCT) dataset

The CERES FluxByCldTyp (FBCT) data product provides daily daytime averages of cloud properties and radiative fluxes, either combined or separated for Terra and Aqua satellites (Wielicki et al., 1995), over a 1° × 1° grid (Eitzen et al., 2017; Sun et al., 2022). We use the CERES Aqua FBCT data from July 2002 to June 2021 (19 years) in this study. These data are stratified by effective cloud ("radiating" top) pressure (p_c) and cloud optical depth (τ) (Rossow & Schiffer, 1999). A cloud type is represented by a p_c - τ pair, that is, the joint distribution of p_c and τ. p_c and τ information is derived from the Moderate Resolution Imaging Spectrometer (MODIS) pixel data with a size of 2 × 2 km^2. A total of 42 discrete cloud types are defined, using seven p_c bins and six τ bins, along with a cloud-free bin. The cloud-free areal fraction is calculated as one minus the sum of cloud fractions across the 42 cloud types.

The microphysical and macrophysical properties of cloud types, such as cloud fraction, cloud liquid water path (LWP), total cloud water path (TCWP; sum of LWP and cloud ice water path, IWP), and effective cloud-top height, are derived from the CERES cloud retrievals of MODIS pixel data (Minnis et al., 2011, 2021). It is important to note that CERES footprints have

a nominal size of 20 × 20 km^2 at nadir, which increases with distance from nadir. To calculate the mean properties for each CERES footprint, each MODIS imager pixel within a CERES footprint is assigned a weight based upon the point spread function of the footprint. The weights are then used to compute cloud fraction and all other cloud parameter values of the footprint.

The algorithm for deriving cloud type-sorted radiative fluxes and clear sky fluxes employs empirically derived narrowband-to-broadband coefficients, converts mean broadband radiances to subfootprint fluxes using CERES angular distribution models (Loeb et al., 2005; Su et al., 2015), and normalizes results against "observed" footprint fluxes (Loeb et al., 2018). The fluxes for each single-scene footprints and subfootprint cloud layers are assigned to their respective $p_c - \tau$ cloud types, and the areal extents of single-scene footprints and subfootprint layers are used to calculate cloud-type averaged fluxes for 1° × 1° grid. Here "single scene" refers to an entire footprint with either a single cloud layer or totally clear skies, while subfootprints are smaller areas of a footprint with either one or two cloud layers (Minnis et al., 2011). Instantaneous shortwave fluxes, including clear sky fluxes, are converted to equivalent daily mean fluxes as detailed in Sun et al. (2022).

The data are averaged over different regions for the 19-year period. Following Takahashi et al. (2017), the five tropical regions are defined as: Africa (0–35°E, 12°S–24°N), Amazon (280–325°E, 15°S–10°N), TWP (90–170°E, 15°S–15°N), East Pacific ITCZ (180–280°E, 0–12°N), and Atlantic ITCZ (310–345°E, 0–12°N). Please refer to Supplementary Information (SI) Figure A1 for the locations of these regions. The entire tropical region is defined as the latitudinal band of 25°S–25°N, which is further subdivided into land and ocean regions based on the land mask.

2.2 Methodology for decomposition of cloud radiative effects

Recently, Xu et al. (2024) derived an expression for the regionally averaged CRE that accounts for the influence of the immediate environment of a specific cloud type. The derivation

of this expression is summarized below. The overall CRE over a region or grid box is traditionally defined as the difference in radiative flux—positive for upward flux—between clear and all skies, with the assumption that clouds are horizontally uniform (Ramanathan et al., 1989). The term "overall CRE" refers to the combined effects of all cloud types within a given region or grid box. Mathematically, CRE is expressed as:

$$CRE = F_{clr} - F_{all} \quad (1),$$

where F is the TOA flux and subscripts *clr* and *all* denote clear skies and all skies, respectively. Eq. (1) can be simplified to the difference between the clear and cloudy fluxes, weighted by cloud fraction, a, as follows:

$$\text{CRE} = F_{clr} - [aF_{cld} + (1-a)F_{clr}] = a(F_{clr} - F_{cld}) \quad (2),$$

where subscript *cld* refers to cloudy skies. If clouds are not horizontally uniform, the overall CRE over a region or grid box is the sum of cloud-type mean CREs multiplied by cloud fraction (CF) across all cloud types. For a specific cloud type j, denoted as $CRE_{cld,j}$, the cloud-type mean CRE is given by the same expression as in (2), but assuming that $a = 1$:

$$CRE_{cld,j} = F_{clr} - F_{cld,j} \quad (3).$$

In Xu et al. (2024), F_{clr} refers to the flux in the environment of cloud type j within a specific 1° × 1° grid of the FBCT data. For regional averages, the regionally averaged cloud-type mean CRE excludes the clear-sky flux from any 1° × 1° grid within the region where the specific cloud type is not present; that is, the regionally averaged F_{clr} is calculated from CF-weighted clear-sky fluxes across all grids. In other word, the simple regional average of all clear sky fluxes weighted by clear-sky area over all grids, which is independent of cloud type, is not used.

The regionally averaged CF-weighted cloud-type mean CREs are summed to obtain the overall CRE across all cloud types, as shown in the following equation:

$$CRE = \sum_{j=1}^{42} \bar{a}_j \, \overline{CRE}_{cld,j} \quad (4),$$

where the overbar denotes the regional average. In the following, we focus on the deviation in the product term on the right-hand side (RHS) of Equation (4) for a specific region compared to the entire tropical region. The product term is called contribution to overall CRE from a cloud type. This term is determined by both regionally averaged cloud-type mean CRE and its CF. By omitting the subscript *j* (for cloud type) and using f to represent the regionally averaged CF and CRE to represent the regionally averaged cloud-type mean CRE, respectively, the difference in the product term on the RHS of Equation (4) between two regions can be expressed as:

$$\begin{aligned} f_1 CRE_1 - f_0 CRE_0 &= (f_0 + \Delta f) \times (CRE_0 + \Delta CRE) - f_0 \times CRE_0 \\ &= f_0 \Delta CRE + \Delta f CRE_0 + \Delta f \Delta CRE \end{aligned} \quad (5),$$

where subscripts 0 and 1 refer to the entire tropical region and a specific region, respectively, and Δ represents the deviation of a specific region from the entire tropical region. The three terms on the RHS of Equation (5) represent the contributions to regional differences in overall CRE from a given cloud type, arising from: (1) the deviation in CRE within a cloud type, (2) the deviation in CF, and (3) the deviations in both CF and CRE. The last term is typically small.

Similar to Bony et al. (2004), Eq. (5) separates changes in overall CRE into two components: those due to CF deviations from those due to CRE deviations within a cloud type. This approach distinguishes the contributions from changes in cloud occurrence and cloud microphysical properties. This decomposition allows for an assessment of the relative importance of CF and CRE deviations in contributing to regional differences in the overall CREs from each cloud type and all types combined. The latter is obtained by summing each individual term on the RHS of Eq. (5) across all 42 cloud types. The results will be shown in Section 3.2.

3. Results

3.1 Tropical mean cloud and radiative properties by cloud type

In this section, we present the tropical-mean cloud fraction and properties and CREs by cloud type, as defined by the joint $p_c - \tau$ distribution. These mean properties serve as a reference for comparing regional differences. For the discussion of results related solely to cloud heights, we use effective cloud-top pressure intervals to classify conventional cloud types: $1000 \geq p_c >$ 800 hPa for boundary-layer clouds, $1000 \geq p_c > 680$ hPa for low-level clouds, $680 \geq p_c > 440$ hPa for mid-level clouds, and $p_c \leq 440$ hPa for high-level clouds. Thin anvils are high-level clouds with $\tau \leq 3.6$ while thick anvils are those with $3.6 < \tau \leq 23$. Note that the definition of boundary-layer clouds is somewhat imprecise, as the heights of the atmospheric boundary layer can vary greatly from ocean to land areas. The deep convective types are defined as the four types in the top-right corner of the $p_c - \tau$ diagrams ($p_c \leq 310$ hPa and $\tau > 23$). Note that cloud types with less than 0.1% area fractions are represented in white to minimize the impact of weak statistics.

For the entire tropical region (Figure 1h), CFs for the 42 cloud types range from less than 1% (accounting for 24 types) to 7.5%, while the clear-sky area fraction is 40.2%. Low- and high-level cloud types with thin-to-moderate optical depths ($\tau \leq 9.4$) are the most abundant, with the largest CF (7.5%) found in one of the boundary-layer cloud types ($1.3 < \tau \leq 3.6$). The CF maximum in the boundary layer is contributed by shallow cumulus and stratocumulus clouds, while the secondary maximum in the upper troposphere (4%) is associated with convective anvils generated by deep convection. The four deep convective types together contribute 2.6%, compared to less than 0.8% from the ten cloud types with lower effective cloud tops but in the same τ range.

Figures 1a-g show the deviations of cloud-type mean CF from the tropical mean (Figure 1h) for both tropical ocean and land regions, as well as the five chimney regions. The contrast

between lands and oceans is pronounced (Figures 1a and 1e); land areas exhibit more mid-level clouds with optical depths of $1.3 < \tau \leq 23$, while oceans have abundance of boundary-layer clouds (1.7%) and slightly more thin anvil clouds (> 0.3%). The deeper planetary boundary layer (PBL) over land (e.g., McGrath-Spangler & Denning, 2013), which is linked to stronger surface heating, explains the absence of low-level cloud types over land (with a maximum deviation of -3.8%) while the abundance of oceanic boundary-layer clouds is attributed to those clouds in the subsidence regions. In contrast, the drier environment over land leads to the evaporation of optically very thin cloud types ($\tau \leq 1.3$). The higher abundance of mid-level clouds over land (maximum deviation of 2.2%) is likely a result of moisture transport from surface, combined with a more unstable atmospheric environment, compared to the concentration of moisture in the lower troposphere over ocean.

The five chimney regions (Figures 1b, c, d, f, g) are overly cloudier than the tropical mean, except for Africa, when summing the CFs across all cloud types. This observation aligns with the findings of Xu et al. (2024), which showed that the magnitudes of the overall SW and LW CREs are greater than the tropical mean. Higher cloud fractions typically lead to more significant SW and LW radiative effects (e.g., Hartmann et al., 1992; Ockert-Bell & Hartmann, 1992), although the precise relationship depends on the cloud type, thickness, altitude, and optical depth. In the following, we will discuss the significant differences in CFs and cloud water paths for individual cloud types among the chimney regions.

The TWP stands out with the highest CFs, with CF deviations peaking at +4.4% for anvil clouds, particularly optically thin ($\tau \leq 3.6$) ones, but it also shows the lowest CFs for boundary-layer clouds, with a maximum deviation of -3.8% (Figure 1b). The absence of low-level clouds in this region can be attributed to high SSTs and the lack of large-scale subsidence. In contrast, the

East Pacific ITCZ region displays a different CF distribution compared to the TWP, with an abundance of low-level clouds (maximum deviation of +1.5%) and optically moderate-to-thick ($3.6 < \tau \leq 60$) mid- and high-level clouds at around +1%. It also has slightly fewer (-0.8%) optically thin clouds ($\tau < 3.6$) compared to the tropical mean (Figure 1c). These differences are consistent with the findings of Kubar et al. (2007), which used a τ-cloud-top temperature joint distribution with MODIS data. The lower SSTs and large-scale subsidence in parts of the East Pacific ITCZ region contribute to the abundance of low-level clouds, while the shorter longevity of mesoscale convective systems relative to those in the TWP helps explain the lack of optically thin clouds.

The Atlantic ITCZ region (Figure 1d) has a CF distribution similar to that of the East Pacific ITCZ region including fewer thin anvil clouds compared to the tropical mean. However, CF deviations for low-level clouds in the Atlantic ITCZ are negative for most cloud types, which are similar to those in the TWP but with smaller amplitudes (-1.6%). Two cloud types with $1.3 < \tau \leq 3.6$ show large positive deviations (+2.2%), associated with the prevalence of cumulus clouds. The absence of stratocumulus clouds ($\tau > 3.6$) in the Atlantic ITCZ compared to the East Pacific ITCZ is likely due to higher SSTs and the lack of large-scale subsidence.

As with the tropical lands (Figure 1e), both the Amazon and Africa regions (Figures 1f, 1g) exhibit relatively abundant mid-level and deep convective clouds but lack boundary-layer clouds (maximum deviations of -4.2% in Africa and -3.0% in the Amazon), attributed to higher PBL heights (e.g., McGrath-Spangler & Denning, 2013). However, Africa has lower CFs for anvil clouds compared to the tropical mean (Figure 1f), likely due to limited moisture availability in the region. In addition, the Amazon exhibits the smallest fraction of optically thin clouds among the five chimney regions, which may indicate shorter lifespans for anvil clouds in this region, possibly resulting from strong diurnal cycles compared to oceanic regions. Another distinct feature of the

320 Amazon region is the abundance of low- and mid-level clouds (+3.7%) between 800-400 hPa,
321 which is likely attributed to relatively wet environments (e.g., Collow et al., 2016).

322 The mean cloud liquid, cloud ice and total water paths (LWP, IWP and TCWP) increase
323 monotonically with τ and decrease with p_c (Figures 2h and 3h). Deep convective cloud types
324 exhibit the highest TCWP, with a maximum of 1900 g m^{-2}. In contrast, the maximum LWP is only
325 390 g m^{-2}, which is associated with a mid-level cloud type. TCWP is presented instead of IWP
326 because deep clouds contain liquid water in the lower troposphere, which is not captured by the
327 passive retrieval algorithm. Specifically, the retrieval algorithm only retrieves IWP for these cloud
328 types due to the single-phase assumption, which is intended to represent the TCWP (Minnis et al.,
329 2011, 2021). Both LWP and IWP are calculated from direct retrievals of τ and droplet radius (r_e)
330 for each pixel from the MODIS radiances. Deviations from the tropical means can be expressed as
331 the sum of relative deviations in τ and r_e, if cloud particle extinction coefficients remain constant.
332 The relative deviation in r_e dominates that of τ because variations in τ within a cloud type are
333 somewhat constrained by the cloud type selection criteria.

334 Deviations in LWP from the tropical mean are generally positive for most oceanic cloud
335 types, with the East Pacific ITCZ region showing the largest positive deviation of 58 g m^{-2} (Figures
336 2a-d). In contrast, land regions tend to have lower LWPs, with deviations of -48 g m^{-2} for tropical
337 land areas (Figure 2e), -66 g m^{-2} for Africa (Figure 2f), and -15.8 g m^{-2} for the Amazon (Figure
338 2g). These lower values are primarily attributed to drier conditions and higher aerosol
339 concentrations. This land-ocean contrast is further explained by deviations in r_e (SI Figure A2),
340 which show negative deviations over land but positive ones over ocean. The smaller contrast
341 between the Amazon and oceanic regions is due to the moist rainforest environment in the
342 Amazon, which is why the Amazon region (Figure 3g) exhibits characteristics more similar to

oceanic regions than to Africa and tropical land areas, which is also reflected in the smaller r_e deviations (SI Figure A2).

Tropical land areas also show higher TCWPs for a few deep convective cloud types compared to tropical ocean areas (Figure 3a and 3e), except for the two thickest cloud types, which exhibit TCWP deviations up to -109 g m^{-2}. This result may be explained by larger extinction coefficients over lands, which are a part of the equation for calculating LWP and IWP (Minnis et al., 2011, 2021). In the five chimney regions (Figures 3b, c, d, f, g), TCWP is generally higher than the tropical mean, except for the TWP region (with a maximum deviation of -66 g m^{-2}), and for the highest/thickest cloud type over Africa (-102 g m^{-2}) and the Amazon (-81 g m^{-2}). However, these deviations are relatively small compared to the mean TCWPs for these cloud types (Figure 3h), meaning that they may have minimal impact to both SW and LW fluxes.

The tropical-mean shortwave (SW), longwave (LW) and net CREs by cloud type and their regional differences are shown in SI Figures A3-A5, which were reproduced from figures shown in Xu et al. (2024). As with LWP and TCWP, the magnitudes of tropical-mean SW CRE increase with τ and decreases with p_c, ranging from slightly positive (1.5 W m^{-2}) for a thin cirrus cloud type to -247.5 W m^{-2} for deep convective clouds (SI Figure A3h). The tropical-mean LW CRE shows similar trends, but with weaker variations in τ and stronger dependencies on p_c, ranging from 2.5 to 175.5 W m^{-2} (SI Figure A4h).

Due to opposing signs between SW and LW CREs, the net CREs are small for most cloud types, except for optically thick low-level clouds ($\tau > 9.4$), which have relatively strong net cooling (SI Figure A5h). Optically thin mid- and high-level clouds ($\tau \leq 9.4$) produce net warming effects, which can offset the net cooling effects of thicker anvils, depending on the relative amounts of CFs. Net CREs range from -120.8 to 50.9 W m^{-2}, with twice as many cloud types showing net

cooling compared to those with net warming, excluding seven cloud types with area fractions less than 0.1%.

Deviations in SW CRE from the tropical mean are generally less than 3 W m^{-2} for most cloud types over tropical oceanic and land areas (SI Figures A3a and A3e). However, the magnitudes of these deviations are much larger in the chimney regions (SI Figures A3b, c, d, f, g). In particular, low-level clouds exhibit weaker cooling effects in the five chimney regions (except the East Pacific) and tropical land areas (SI Figure A3e). High-level and deep convective clouds show stronger cooling over oceans but weaker cooling over land regions. The weaker cooling effects for low-level clouds over land may result from a combination of (1) increased reflection from clear skies and (2) lower LWP values (Figures 2e-g and SI Figures A3e-g). In the Atlantic region, the lower LWPs are likely the primary cause (Figures 2d and SI Figure A3d).

Deviations in LW CRE from the tropical mean (SI Figures A4a-g) are mostly negative, indicating reduced LW warming, except for a few optically thin cloud types over tropical lands and Africa. The tropical ocean region shows weak enhancement in LW warming particularly for mid- and high-level clouds. The overall reduction in LW warming for nearly all cloud types is linked to more humid environments outside of clouds compared to the relatively drier conditions over clear skies in less convectively active regions (Xu et al., 2024).

Deviations in net cloud cooling effects (SI Figures A5a-g) exhibit patterns similar to those of SW cloud cooling (SI Figures A3a-g). However, net cloud cooling effects are greater than SW cooling effects in all regions due to the weaker LW warming (SI Figure A4a-g). For instance, while SW cloud cooling over the Amazon is smaller than the tropical mean, net cloud cooling exceeds the tropical mean for most cloud types, except for a few low-level cloud types (SI Figures A4g and A5g).

3.2 Decomposition of cloud radiative effects

Xu et al. (2024) showed that the overall LW warming and SW cooling in the chimney regions, except for Africa, are stronger than the tropical mean. This result does not stem from the deviations in cloud-type mean LW and SW CREs discussed earlier (SI Figures A3 and A4). In fact, most cloud types exhibit weaker LW warming than the tropical mean, and SW cooling is only stronger in the East Pacific and for a few cloud types in the TWP and Atlantic regions. This apparent discrepancy can be explained by the decomposition components outlined in Section 2.2: (1) deviations in CRE within a cloud type, (2) deviations in CF, and (3) the combined deviations. In the following, we discuss the results for these three components. Plots for tropical ocean and land areas are included for completeness, although these results are only briefly discussed below due to their smaller magnitudes compared to those of the chimney regions.

Figures 4, 5 and 6 present the three components of LW CRE decomposition. The CRE deviation component (Figure 4) closely mirrors the LW CRE deviation (see SI Figures A4a-g), though with some noticeable differences. Specifically, the magnitudes for anvil clouds in the 310 $\geq p_c >$ 100 hPa layer and for boundary-layer clouds are relatively larger compared to other cloud types, due to the larger CF magnitudes in these two layers over the entire tropical region (Figure 1h). The maximum contribution of any individual cloud type to regional differences in overall LW CRE ranges from a reduction of 0.2 W m^{-2} (TWP) to 0.5 W m^{-2} (Amazon). Despite the small magnitudes for individual cloud types, the 42 cloud types collectively reduce the overall LW CRE warming by just over 2 W m^{-2} across the five chimney regions, with slightly larger reductions in the Atlantic (2.9 W m^{-2}) and Amazon (3.5 W m^{-2}).

The sign of the CF deviation (Figures 1a-g) determines the sign of the CF deviation component, while its magnitude increases as p_c decreases (Figure 5). This trend is influenced by

412 the tropical-mean LW CRE (SI Figure A4h), which increases as p_c decreases. Except for a few
413 cloud types showing weak cooling due to negative CF deviations (Figures 1a-g), the CF deviation
414 component generally enhances LW cloud warming for most cloud types in chimney regions and
415 tropical land areas (Figures 5b-g), due to positive CF deviations (Figures 1b-g).

416 Compared to the CRE deviation component, the magnitudes in the CF deviation component
417 are roughly an order of magnitude larger. [Note that the color bar range in Figure 5 is five times
418 that of Figure 4.] For instance, the maximum contribution of any individual cloud type to regional
419 differences in overall LW CRE ranges from 0.6 W m^{-2} (Africa), 1.3 W m^{-2} (East Pacific), 1.5 W
420 m^{-2} (Atlantic), 2.3 W m^{-2} (Amazon), to 5.0 W m^{-2} (TWP). These maxima are associated with thick
421 anvil and deep convective cloud types in all regions (Figures 5b, c, d and g) except for Africa
422 (from mid-level clouds). In contrast, there are only a few cloud types in each region contributing
423 to a reduction in LW warming, with maximum magnitudes between -0.3 and -0.5 W m^{-2}.
424 Collectively, the 42 cloud types increase overall LW CRE warming by 20.4 W m^{-2} in the TWP,
425 11.7 W m^{-2} in the Amazon, 5.1 W m^{-2} in the East Pacific and Atlantic ITCZ regions and 2.7 W m^{-2}
426 in the tropical land areas, with no increase observed in Africa. The increase in the overall LW
427 CRE warming is primarily driven by high-level cloud types in these regions, with the largest
428 warming corresponding to the highest CF deviations in the TWP. The absence of an increase in
429 Africa is attributed to the cancellation of effects from mid-level clouds (positive) with boundary-
430 layer and upper-tropospheric clouds (negative).

431 The third component, which accounts for both CF and CRE deviations, exhibits smaller
432 magnitudes overall but is comparable to the CRE deviation component in the TWP and Amazonia
433 regions, where the maximum reduction in LW cloud warming is about 0.25 W m^{-2}. Overall, the
434 reduction in LW cloud warming is minimal across the five chimney regions, with the exceptions

435 of the TWP (-0.8 W m^{-2}) and Amazonia (-1.8 W m^{-2}). The larger reduction in the Amazonia region
436 compared to the TWP is attributed to the stronger cooling effects of optically moderate cloud types
437 associated with positive CF deviations (Figure 1g).

438 Figures 7, 8 and 9 show the three components of SW CRE decomposition. As in the LW
439 CRE decomposition, the magnitudes of the CF deviation component for each cloud type are
440 considerably larger than those of the CRE deviation component, which in turn are larger than the
441 combined component of both CF and CRE deviations. In terms of their contribution to
442 enhancement or reduction of overall SW cloud cooling, regional differences are much more
443 pronounced compared to the LW CRE decomposition, as will be discussed below.

444 The sign of the SW CRE deviation component (Figure 7) mirrors the SW CRE deviation
445 itself (SI Figures A3a-g). It reduces SW cloud cooling for nearly all cloud types in the Africa and
446 Amazonia regions, as well as for low-level cloud types in the TWP and Atlantic regions.
447 Conversely, it enhances SW cloud cooling for nearly all cloud types in the East Pacific region and
448 for high-level clouds in the TWP and Atlantic regions. The maximum contribution of any
449 individual cloud type to enhancing overall SW cloud cooling is less than -0.26 W m^{-2} across the
450 five chimney regions. Contributions to reducing overall SW cloud cooling, primarily from
451 boundary-layer clouds, are slightly larger: 0.34 W m^{-2} in the TWP, 0.81 W m^{-2} in the Atlantic, 0.58
452 W m^{-2} in Africa, 0.45 W m^{-2} in the Amazon and 0.61 W m^{-2} in tropical land areas. Collectively,
453 the 42 cloud types reduce overall SW cloud cooling in all chimney regions except the East Pacific,
454 where it enhances by -2.2 W m^{-2}. Specifically, reductions in overall SW cooling are less than 1 W
455 m^{-2} in the TWP and Atlantic, 2.0 W m^{-2} in the Amazon and 3.5 W m^{-2} in Africa.

456 The SW CF deviation component (Figure 8) generally enhances cloud cooling for most
457 cloud types, except for most low-level clouds in the TWP, Atlantic and Africa regions, as well as

458 boundary-layer clouds in the Amazon and tropical land regions. That is, positive (negative) CF
459 deviations enhance (diminish) SW cloud cooling (Figures 1a-g; 8a-g). The degree of enhancement
460 or reduction of any individual cloud type to overall SW cloud cooling varies significantly between
461 regions. The maximum contribution to enhancement of overall SW cloud cooling ranges from -
462 0.84 W m^{-2} in Africa, -1.7 W m^{-2} in tropical land areas, -1.8 W m^{-2} in the East Pacific, -2.1 W m^{-2}
463 in the Atlantic, -2.9 W m^{-2} in the Amazon, to -4.8 W m^{-2} in the TWP. The maximum contribution
464 to cooling reduction ranges from 0.2 W m^{-2} in the East Pacific to 2.4 W m^{-2} in the TWP. Unlike
465 its LW counterpart, there is no systematic dependence of the absolute magnitude on p_c within a
466 given region. In general, the 42 cloud types contribute to strengthening overall SW cloud cooling
467 across all regions, except for Africa, which experiences a reduction of 2.5 W m^{-2}. Enhancements
468 in overall SW cloud cooling in the chimney regions compared to the tropical mean range from -
469 6.1 W m^{-2} in the Atlantic, -10.9 W m^{-2} in the East Pacific, -13.9 W m^{-2} in the TWP, to -18.3 W m^{-2}
470 in the Amazon. Optically moderate-to-thick clouds (with various p_c) are the primary drivers of
471 these enhanced SW cooling effects, except in Africa.

472 The third SW CRE component (Figure 9) also show relatively small effect. Most of cloud
473 types, including anvil clouds and boundary-layer clouds, enhance cooling across all regions except
474 the Amazon. The collective contributions from the 42 cloud types range from -0.9 W m^{-2} in the
475 TWP to 0.6 W m^{-2} in the Amazon, which are even smaller than those of the CRE deviation
476 component discussed earlier.

477 Figures 10 and 11 present the CRE and CF deviation components of the net CRE
478 decomposition, respectively. The combined component, which is not shown but can be derived
479 from the summation of Figures 6 and 9, has a minimal effect. Exceptions to this are observed in
480 anvil clouds in the TWP, East Pacific and Atlantic regions.

481 The net CRE deviation component (Figure 10) closely resembles its counterpart in the SW
482 CRE decomposition (Figure 7) except for larger magnitudes of enhanced cooling due to the LW
483 component (Figure 4). It enhances net cloud cooling for nearly all cloud types in the TWP, East
484 Pacific, Atlantic and Amazon, except for boundary-layer clouds in the TWP and Amazon and
485 optically thin low-level clouds in the Atlantic. In Africa, this component produces weaker net
486 cloud warming compared to its SW counterpart (Figures 7f and 10f). The maximum contribution
487 to the enhancement or reduction of overall net cloud cooling from any individual cloud type range
488 from -0.5 to 0.6 W m^{-2} across all regions, which is smaller than the corresponding values in the
489 SW CRE decomposition. Collectively, the 42 cloud types contribute to a reduction in overall net
490 cloud cooling by 1.5 W m^{-2} in Africa, while enhancing net cloud cooling by -1.5 W m^{-2} in the
491 Amazon, -2.0 W m^{-2} in the Atlantic, -2.2 W m^{-2} in the TWP, and -4.4 W m^{-2} in the East Pacific.

492 The CF deviation component in the net CRE decomposition (Figure 11) differ significantly
493 from that in the SW CRE decomposition (Figure 8), as the enhanced cooling in the upper
494 troposphere seen in the SW CRE decomposition largely disappears due to the near cancellation
495 between LW and SW CREs. This results in relatively small tropical-mean net CREs (SI Figure
496 A5h). For other cloud types, the sign of this component depends on both the signs of CF deviations
497 (Figure 1) and tropical-mean net CRE (SI Figure A5h). The maximum contribution to the
498 enhancement of overall net cooling from any individual cloud type ranges from -0.35 W m^{-2} in
499 Africa, -0.67 W m^{-2} in the Atlantic, -0.85 W m^{-2} in the TWP and East Pacific, to -2.10 W m^{-2} in
500 the Amazon. These values are mostly associated with either optically thick high-level clouds (TWP
501 and Atlantic) or low-level clouds (East Pacific, Amazon, and tropical land areas). Boundary-layer
502 or low-level clouds, with values ranging from 0.90 W m^{-2} in the Amazon, 1.0 W m^{-2} in the Atlantic,
503 1.1 W m^{-2} in Africa, 1.8 W m^{-2} in tropical lands, to 2.1 W m^{-2} in the TWP, contribute to the

reduction of overall net cooling, except in the East Pacific. The East Pacific is unique in exhibiting enhanced low-level CF and net cooling, in contrast to other regions (Figures 1a-g). In addition, reductions in net cloud cooling from thin anvil clouds are observed in the TWP, linked to large positive CF deviations in that region (Figure 1b).

Collectively, the 42 cloud types contribute to a reduction of overall net cloud cooling by 2.5 W m^{-2} in Africa and 6.5 W m^{-2} in the TWP, due to the lack of low-level clouds and/or an abundance of thin anvil clouds (the TWP). In contrast, the overall net cloud cooling is enhanced by -1.0 W m^{-2} in the Atlantic, -5.8 W m^{-2} in the East Pacific and -7.1 W m^{-2} in the Amazon, due to the prevalence of optically thick clouds and/or an abundance of low- and mid-level clouds. It is important to note that regional variations in overall net CREs from the CF deviation component, ranging from -7.1 to 6.5 W m^{-2}, closely align with those observed in the net CRE deviation component, which spans from -4.4 to 1.2 W m^{-2}. This underscores the nearly equal importance of both deviation components in influencing regional differences in overall net CREs.

Figure 12 summarizes the overall CRE differences from the tropical mean based on the decomposition analysis. Xu et al. (2024) showed that the magnitudes of regional-averaged LW and SW CREs are generally larger than the tropical mean for all chimney regions, except for Africa. From this analysis, these regional variations are primarily driven by the CF deviation component, rather than the CRE deviation component, as the increased cloudiness, particularly upper-tropospheric clouds, enhances the magnitudes of both SW and LW CRE (Figures 12a, b). As shown in Figures 1a-g, these regions are much cloudier than the tropical mean, particularly for the TWP and Amazon, which exceed the tropical mean LW and SW CREs by 10-20 W m^{-2}.

Another key finding from Xu et al. (2024) is that net cloud cooling (i.e., net CRE) varies across regions: enhanced cooling of approximately 9 W m^{-2} in the East Pacific and Amazon, and

2.4 W m^{-2} in the Atlantic, but less cooling of 0.6 W m^{-2} in the TWP and 3.4 W m^{-2} in Africa. This analysis shows that these regional variations depend on those in the distribution of cloud types. The large net cooling in the East Pacific and Amazon is attributed to an increase in optically thick clouds, while the relatively small net warming in the TWP is due to the dominance of enhanced thin anvil clouds. Other key findings of this study include that in the East Pacific, Atlantic and Africa, both CF and CRE deviation components contribute nearly equally, while in the Amazon, the CF component dominates, and in the TWP, the two components exhibit opposite signs with a smaller contribution from the combined deviations (Figure 12c). These regional differences are likely attributed to variations in cloud properties and environmental conditions that affect both CF and CRE deviations across different cloud types.

4 Summary and discussion

This study examines a 19-year mean of cloud properties and their radiative effects (CREs) by cloud type, focusing on regional variations across convectively active tropical regions. The analysis utilizes the CERES FluxByCldTyp (FBCT) data product (Sun et al., 2022), which provides daily daytime averages of cloud properties and radiative fluxes over a 1° × 1° grid for 42 cloud types, categorized based on effective cloud-top pressure and cloud optical depth. The analysis covers the chimney regions of the Tropical Western Pacific (TWP), East Pacific and Atlantic ITCZs, equatorial Africa, and the Amazon, along with broader tropical ocean and land areas.

The study reveals significant regional differences in cloud fraction (CF) and microphysical properties, which can impact the precise relationships between clouds and their radiative effects. Oceanic regions are predominantly characterized by convective anvils and boundary-layer clouds, which have higher liquid and ice water contents. In contrast, land regions show higher fractions of

mid-level clouds with lower liquid water contents, related to the scarcity of moisture and deeper PBLs. In the five chimney regions, CFs are above the tropical mean, with the TWP having the highest proportion of anvil clouds and the lowest of boundary-layer clouds. The East Pacific and Atlantic ITCZs show different cloud distributions, with abundant boundary-layer (cumulus only in Atlantic) clouds and fewer optically thin clouds. These differences across the oceanic regions are linked to variations in SSTs and atmospheric stability driven by large-scale dynamics. On land, the relative absence of boundary-layer clouds is due to higher PBL tops, which limit cloud formation below 800 hPa, but mid- and high-level clouds are abundant in Africa and the Amazon due to stronger atmospheric instability related to daytime surface heating. The Amazon, unlike Africa, exhibits more mid- and high-level clouds with relatively higher cloud water, similar to oceanic regions, which is attributed to its wetter environment.

The study explores how cloud distribution and properties influence shortwave (SW), longwave (LW) and net CREs, breaking down the contributions to regional differences in overall CRE from individual cloud types into three components: deviations in CRE within a cloud type, CF, and both combined, relative to the tropical means. The "overall" CRE refers to the combined effects of all cloud types within a given region. The key finding is that the magnitudes of CF deviation-driven effects, which either enhance or reduce LW, SW and net CREs depending on cloud type, are considerably larger than the contributions from CRE deviations within a cloud type and combined CF and CRE deviations. This suggests that CF deviations alone largely account for the regional variations in CRE for most cloud types. As a result, cloud distribution, in terms of departures from the tropical mean, becomes a crucial factor in determining the overall CREs, particularly net CRE, due to the stark differences in LW, SW and net CREs between low- and high-level clouds, as well as between optically thin and moderate/thick clouds. This helps explain

why the overall net cloud cooling in the East Pacific and Amazon are much stronger than the TWP even though the TWP is overly cloudier than both regions. The abundance of thin anvils in the TWP leads to net cloud radiative warming, contributing to a nearly zero net CRE for all cloud types combined (Hartmann & Berry, 2017; Hartmann et al., 1992; Kiehl, 1994).

Another key finding is that, although the CRE deviation component is smaller than the CF deviation component for individual cloud types, it has a more significant impact on regional CRE differences when all types are considered together, particularly for net CRE. This is because the CF deviation component exhibits opposing effects between low- and high-level clouds, while the CRE deviation component shows more consistent regional differences across all cloud types. The CRE deviation component consistently reduces LW warming across all chimney regions, although its effects on SW and net CREs vary regionally. This component has often been overlooked in previous studies (e.g., Hartmann and Berry 2017; Hartmann et al., 1992; Hill et al., 2018; Kubar et al., 2007; Lin et al., 2010; Ockert-Bell & Hartmann, 1992; Xu et al., 2023), which could have important implications for cloud feedback analysis (e.g., Ceppi & Nowack, 2021; Raghuraman et al., 2023, 2024; Randall et al., 2007; Stephens, 2005; Vial et al., 2013).

Significant regional differences in cloud-type mean properties and CREs, as revealed from this study, can arise from land-ocean contrasts and local meteorological conditions. Boundary-layer clouds are influenced by atmospheric stability, which is driven by large-scale dynamics, as well as the PBL thickness, both of which directly impact the strength of convective clouds. In contrast, mid- and high-level clouds over lands, particularly in Africa, are likely influenced by higher atmospheric instability driven by elevated surface heating, though moisture availability limits their extent. The Amazon region, with its relatively high cloud liquid water and stronger net cooling effects, suggest more robust convective systems, sustained by higher aerosol

concentrations from both natural and anthropogenic sources in a moist environment, though the strong diurnal cycle limits the lifespans of convective anvils in this region. However, it is beyond the scope of this study to fully explore the relationships of these factors and their influence on regional differences in cloud properties and CREs.

In conclusion, this study provides valuable insights into the 19-year mean of tropical cloud properties and their radiative effects among different cloud types. These findings have important implications for understanding cloud-climate feedback in the tropics and highlight the need for future research on temporal variability of cloud types and their interactions with atmospheric circulations to better predict the impacts of climate change on tropical clouds.

Acknowledgments. This work has been supported by NASA Science of Terra, Aqua, and NPP program (KX and YZ) and the NASA CERES project (MS).

Data Availability Statement. The CERES FluxByCldTyp (FBCT) Level 3 data product is publicly available and can be accessed via CERES data portal (https://ceres.larc.nasa.gov/data/). The regionally averaged daily FBCT data are in the Zenodo database (Sun & Xu, 2024).

References

Bony, S., & Dufresne, J.-L., (2005). Marine boundary layer clouds at the heart of tropical cloud feedback uncertainties in climate models. *Geophys. Res. Lett., 23*, L20806, doi:10.1029/2005GL023851.

Bony, S., Dufresne, J.-L., Le Treut, H., Morcrette, J.-J., & Senior, C., (2004). On dynamic and thermodynamic components of cloud changes. *Climate Dyn., 22(2-3),* 71–86. https://doi.org/10.1007/s00382-003-0369-6.

Burleyson, C. D., Long, C. N., Comstock, J. M., (2015). Quantifying diurnal cloud radiative effects by cloud type in the tropical western Pacific. *J. Appl. Meteor. Climatol., 54,* 1297–1312.

Ceppi, P., & Nowack, P., (2021). Observational evidence that cloud feedback amplifies global warming. *Proc. Nat. Acad. Sci., 118,* e2026290118. https://doi.org/10.1073/pnas.2026290118.

Collow, A. B. M., Miller, M. A., & Trabachino, L. C., (2016). Cloudiness over the Amazon rainforest: Meteorology and thermodynamics. *J. Geophys. Res. Atmos., 121,* 7990–8005, doi:10.1002/2016JD024848.

Eitzen, Z. A., Su, W., Xu, K.-M., Loeb, N., Sun, M., Doelling, D. R., et al., (2017). Evaluation of a general circulation model by the CERES Flux-by-Cloud Type simulator. *J. Geophys. Res. Atmos., 122,* 10655–10668. https://doi.org/10.1002/2017JD027076.

Feng, Z., Dong, X., Xi, B., Schumacher, C., Minnis, P., & Khaiyer, M., (2011). Top-of-atmosphere radiation budget of convective core/stratiform rain and anvil clouds from deep convective systems. *J. Geophys. Res., 116*, D23202, doi:10.1029/2011JD016451.

Hang, Y, L'Ecuyer, T. S., Henderson, D. S., Matus, A. V., & Wang, Z., (2019). Reassessing the effect of cloud type on Earth's energy balance in the age of active spaceborne observations. Part II: Atmospheric heating. *J. Climate, 32,* 6219–6236. https://doi.org/10.1175/JCLI-D-18-0754.1.

Hartmann, D. L. & Berry, S. E., (2017). The balanced radiative effect of tropical anvil clouds, *J. Geophys. Res. Atmos., 122,* 5003-5020. https://doi.org/10.1002/2017JD026460.

Hartmann, D. L., Okhert-Bell, M. E., & Michelson, M. L., (1992). The effect of cloud type on Earth's energy balance: Global analysis. *J. Climate, 5(11),* 1281–1304. https://doi.org/10.1175/1520-0442(1992)005<1281:teocto>2.0.co;2.

Hill, P. G., Allan, R. P., Chiu, J. C., Bodas-Salcedo, A., & Knippertz, P., (2018). Quantifying the contribution of different cloud types to the radiation budget in southern West Africa. *J. Climate, 31,* 5273-5291. https://doi.org/10.1175/JCLI-D-17-0586.1.

Kiehl, J. T., (1994). On the observed near cancellation between longwave and shortwave cloud forcing in tropical regions. *J. Climate, 7(4),* 559–565. https://doi.org/10.1175/1520-0442(1994)007<0559:otoncb>2.0.co;2.

Kubar, T. L., Hartmann, D. L., & Wood, R., (2007). Radiative and convective driving of tropical high clouds. *J. Climate, 20,* 5550-5526. https://doi.org/10.1175/2007JCLI1628.1.

L'Ecuyer, T. S., Hang, Y., Matus, A. V., & Z. Wang, Z., (2019). Reassessing the effect of cloud type on Earth's energy balance in the age of active spaceborne observations. Part I: Top of atmosphere and surface. *J. Climate, 32,* 6219–6236. https://doi.org/10.1175/JCLI-D-18-0753.1.

LeMone, M. A., & Zipser, E. J. (1980). Cumulonimbus vertical velocity events in GATE. Part I: Diameter, intensity and mass flux. *J. Atmos. Sci., 37(11),* 2444–2457. https://doi.org/10.1175/1520-0469(1980)037<2444:cvveig>2.0.co;2.

Lin, B., Minnis, P., Fan, T. F., Hu, Y., & Sun, W. (2010). Radiation characteristics of low and high clouds in different oceanic regions observed by CERES and MODIS. *International J. Remote Sens., 31(24),* 6473–6492. https://doi.org/10.1080/01431160903548005.

Loeb, N. G., Kato, S., Loukachine, K., and Manalo-Smith, N., (2005). Angular distribution models for top-of-atmosphere radiative flux estimation from the Clouds and the Earth's Radiant Energy System instrument on the Terra satellite. Part I: Methodology. *J. Atmos. Ocean. Tech., 22,* 338–351. https://doi.org/10.1175/JTECH1712.1.

Loeb, N. G., Doelling, D. R., Wang, H., Su, W., Nguyen, C., Corbett, J. G., et al., (2018). Clouds and the Earth's Radiant Energy System (CERES) Energy Balanced and Filled (EBAF) Top-of-Atmosphere (TOA) Edition-4.0 data product. *J. Climate, 31,* 895–918. https://doi.org/10.1175/JCLI-D-17-0208.1.

Lucas, C., Zipser, E. J., & LeMone, M. A., (1994). Convective available potential energy in the environment of oceanic and continental clouds: Correction and comments. *J. Atmos. Sci., 51,* 3829–3830. https://doi.org/10.1175/1520-0469(1994)051<3829:capeit>2.0.co;2.

Luo, H., Quaas, J., & Han, Y., (2023). Examining cloud vertical structure and radiative effects from satellite retrievals and evaluation of CMIP6 scenarios. *Atmos. Chem. Phys., 23,* 8169–8186. https://doi.org/10.5194/acp-23-8169-2023.

Mapes, B. E., (1993). Gregarious tropical convection. *J. Atmos. Sci., 50,* 2026–2037,

McGrath-Spangler, E. L., and Denning, A. S., (2013). Global seasonal variations of midday planetary boundary layer depth from CALIPSO space-borne LIDAR. *J. Geophys. Res. Atmos., 118,* 1226–1233. https://doi.org/10.1002/jgrd.50198.

Minnis, P., Sun-Mack, S., Young, D. F., Heck, P. W., Garber, D. P., Chen, Y., et al., (2011). CERES Edition-2 cloud property retrievals using TRMM VIRS and Terra and Aqua

MODIS data—Part I: Algorithms. *IEEE Trans. Geosci. Remote Sens.,* 49(11), 4374–4400. https://doi.org/10.1109/TGRS.2011.2144601.

Minnis, P., Sun-Mack, S., Young, D. F., Heck, P. W., Garber, D. P., Chen, Y., et al., (2021). CERES MODIS cloud product retrievals for edition 4—Part I: Algorithm changes. *IEEE Trans. Geosci. Remote Sens., 59(4),* 2744-2780. https://doi.org/10.1109/TGRS.2020.2008866.

Najarian, H., & Sakaeda, N., (2023). The influence of cloud types on cloud-radiative forcing during DYNAMO/AMIE. *J. Geophys. Res. Atmos., 128, e2022JD038006. https://doi.org/10.1029/2002JD038006.*

Ockert-Bell, M. E., Hartmann, D. L., (1992). The effect of cloud type on Earth's energy balance: Results for selected regions. *J. Climate, 5,* 1157-1171. https://doi.org/10.1175/1520-0442(1992)005<1157:TEOCTO>2.0.CO;2.

Pilewskie, J., Stephens, G., Takahashi, H., & L'Ecuyer, T., (2024). A multi-satellite perspective on "Hot Tower" characteristics in the equatorial trough zone. *Surv. Geophys*., 45, 1933–1958. https://doi.org/10.1007/s10712-024-09868-2.

Raghuraman, S. P., Medeiros, B., & Gettelman, A., (2024). Observational quantification of tropical high cloud changes and feedbacks. *J. Geophy. Res. Atmos., 129(7),* e2023JD039364. https://doi.org/10.1029/2023JD039364.

Raghuraman, S. P., Paynter, D., Menzel, R., & Ramaswamy, V. ,(2023). Forcing, cloud feedbacks, cloud masking, and internal variability in the cloud radiative effect satellite record. *J. Climate, 36(12),* 4151–4167. https://doi.org/10.1175/jcli-d-22-0555.1.

Ramanathan, V., Cess, R. D., Harrison, E. F., Minnis, P., Barkstrom, B. R., Ahmad, E., and Hartmann, D., (1989). Cloud-radiative forcing and climate: Results from the Earth Radiation Budget Experiment. *Science, 243,* 57–63.

Randall, D. A., et al., (2007). Climate models and their evaluation, in Climate Change 2007: The Physical Science Basis. Contribution of Working Group I to the Fourth Assessment Report of the Intergovernmental Panel on Climate Change, pp. 589–662, Cambridge Univ. Press, Cambridge, U. K.

Riehl, H., & Malkus, J. S., (1958). On the heat balance in the equatorial trough zone. *Geophysica*, *6*, 503–538.

Riehl, H., & Simpson, J. S., (1979). The heat balance of the equatorial trough zone, revisited. *Contrib. Atmos. Phys.*, *52*, 287–305.

Rossow, W. B., & Schiffer, R. A., (1999). Advances in understanding clouds from ISCCP. *Bull. Amer. Meteor. Soc., 80,* 2261–2287.

Stephens, G. L., (2005), Cloud feedbacks in the climate system: A critical review. *J. Climate, 18,* 237-273. https://doi.org/10.1175/JCLI-3243.1.

Su, W., Corbett, J., Eitzen, Z., and Liang, L., (2015). Next-generation angular distribution models for top-of-atmosphere radiative flux calculation from CERES instruments: methodology. *Atmos. Meas. Tech., 8,* 611–632. https://doi.org/10.5194/amt-8-611-2015.

Sun, M., & Xu, K.-M., (2024). FluxByCldTyp Ed4 19 years of regional averaged data [Dataset]. Zenodo. https://doi.org/10.5281/zenodo.13527103.

Sun, M., Doelling, D. R., Loeb, N. G., Scott, R. C., Wilkins, J., Nguyen, L. T., & Mlynczak, P., (2022). Clouds and the Earth's radiant energy system (CERES) FluxByCldTyp edition 4 data product. *J. Atmos. Oceanic Tech., 39,* 303–318. https://doi.org/10.1175/JTECH-D-21-0029.1.

Takahashi, H., Luo, Z. J., & Stephens, G. L. (2017). Level of neutral buoyancy, deep convective outflow, and convective core: New perspectives based on 5 years of CloudSat data. *J. Geophys. Res. Atmos., 122,* 2958–2969, doi:10.1002/2016JD025969.

Takahashi, H, Luo, Z. J., Stephens, G. L., & Mulholland, J. P., (2023). Revisiting the land-ocean contrasts in deep convective cloud intensity using global satellite observations. *Geophys. Res. Lett., 50,* e2022GL102089. https://doi.org/10.1029/2022GL102089

Vial, J., Dufresne, J.-L., & Bony, S., (2013). On the interpretation of inter-model spread in CMIP5 climate sensitivity estimates. *Clim. Dyn., 41,* 3339–3362, doi:10.1007/s00382-013-1725-9.

Wielicki, B. A., Harrison, E. F., Cess, R. D., King, M. D. & Randall, D. A., (1995). Mission to planet earth: role of clouds and radiation in climate. *Bull. Amer. Meteor. Soc., 76,* 2125-2153.

Wielicki, B. A., Barkstrom, B. R., Harrison, E. F., Lee, R. B., Smith, G. L., & Cooper, J. E., (1996). Clouds and the Earth's Radiant Energy System (CERES): An Earth Observing System experiment, *Bull. Am. Meteor. Soc., 77,* 853–868.

Williams, E., & Stanfill, S. (2002). The physical origin of the land–ocean contrast in lightning activity. *C. R. Physique, 3,* 1277–1292. https://doi.org/10.1016/s1631-0705(02)01407-x.

Xu, K.-M., & Cheng A., (2016). Understanding the tropical cloud feedback from an analysis of the circulation and stability regimes simulated from an upgraded multiscale modeling framework. *J. Adv. Model. Earth Syst., 8,* 1825–1846, doi:10.1002/2016MS000767.

Xu, K.-M., & Randall, D. A., (2001). Updraft and downdraft statistics of simulated tropical and midlatitude cumulus convection. *J. Atmos. Sci., 58,* 1630–1649.

Xu, K.-M., Zhou, Y., Sun, M., Kato, S., & Hu, Y., (2023). Observed cloud type-sorted cloud property and radiative flux changes with the degree of convective aggregation from CERES data. *J. Geophys. Res. Atmos., 128,* e2023JD039152. https://doi.org/10.1029/2023JD039152.

Xu, K.-M., Sun, M., & Zhou, Y., (2024). Analysis of the influence of clear-sky fluxes on the cloud-type mean cloud radiative effects in the tropical convectively active regions with CERES satellite data. *J. Geophys. Res. Atmos., 129,* e2024JD041525. https://doi.org/10.1029/2024JD041525.

Yuan, J., Hartmann, D. L., & Wood, R., (2008). Dynamic effects on the tropical cloud radiative forcing and radiation budget. *J. Climate, 21,* 2337-2351. https://doi.org/10.1175/2007JCLI1857.1.

Zhao, M., (2024). Cloud radiative effects associated with daily weather regimes. *Geophys. Res. Lett., 51,* e2024GL109090. https://doi.org/10.1029/2024GL109090.

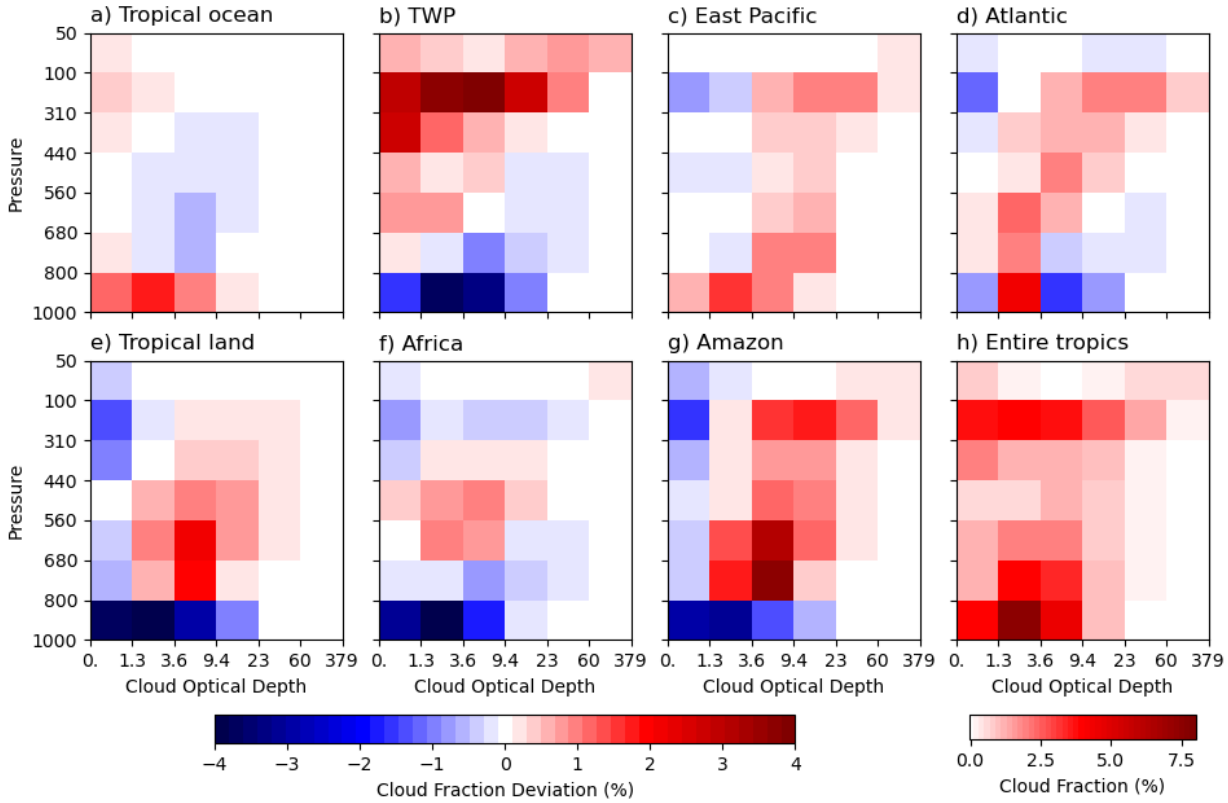

Figure 1. The cloud-type (p_c- τ) mean cloud fraction (g) and the deviation in cloud-type (p_c- τ) mean cloud fraction from the entire tropical region (25°N - 25°S) for (a) the entire tropical ocean, (b) the Tropical Western Pacific (TWP), (c) the East Pacific and (d) Atlantic intertropical convergence zones (ITCZs), (e) the entire tropical land, (f) Africa and (g) Amazonia regions. Cloud type is classified based on the joint distribution of effective cloud-top pressure (p_c) and cloud optical depth (τ). See texts for the latitudinal and longitudinal bounds of these regions. Unit is %.

812

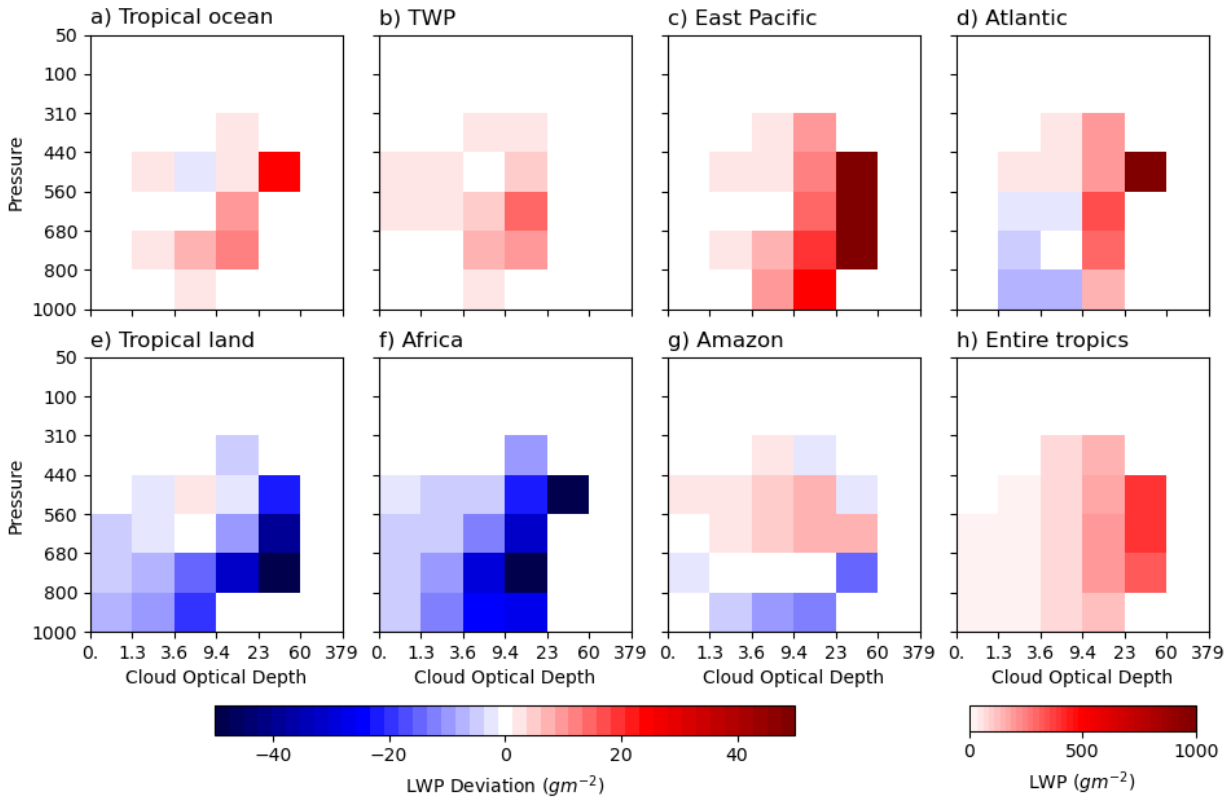

Figure 2. As in Figure 1, except for cloud liquid water path (LWP). Unit is g m^{-2}.

813
814

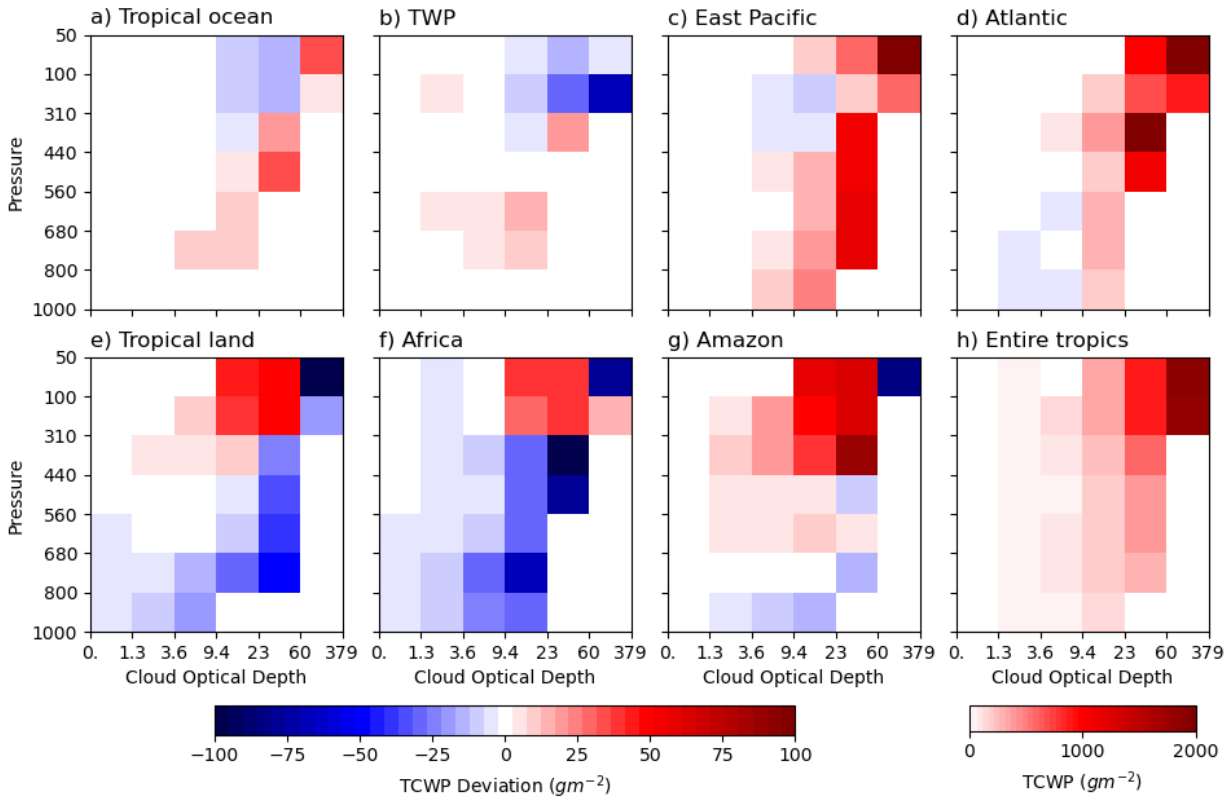

Figure 3. As in Figure 1, except for total cloud (liquid + ice) water path (TCWP). Unit is g m^{-2}.

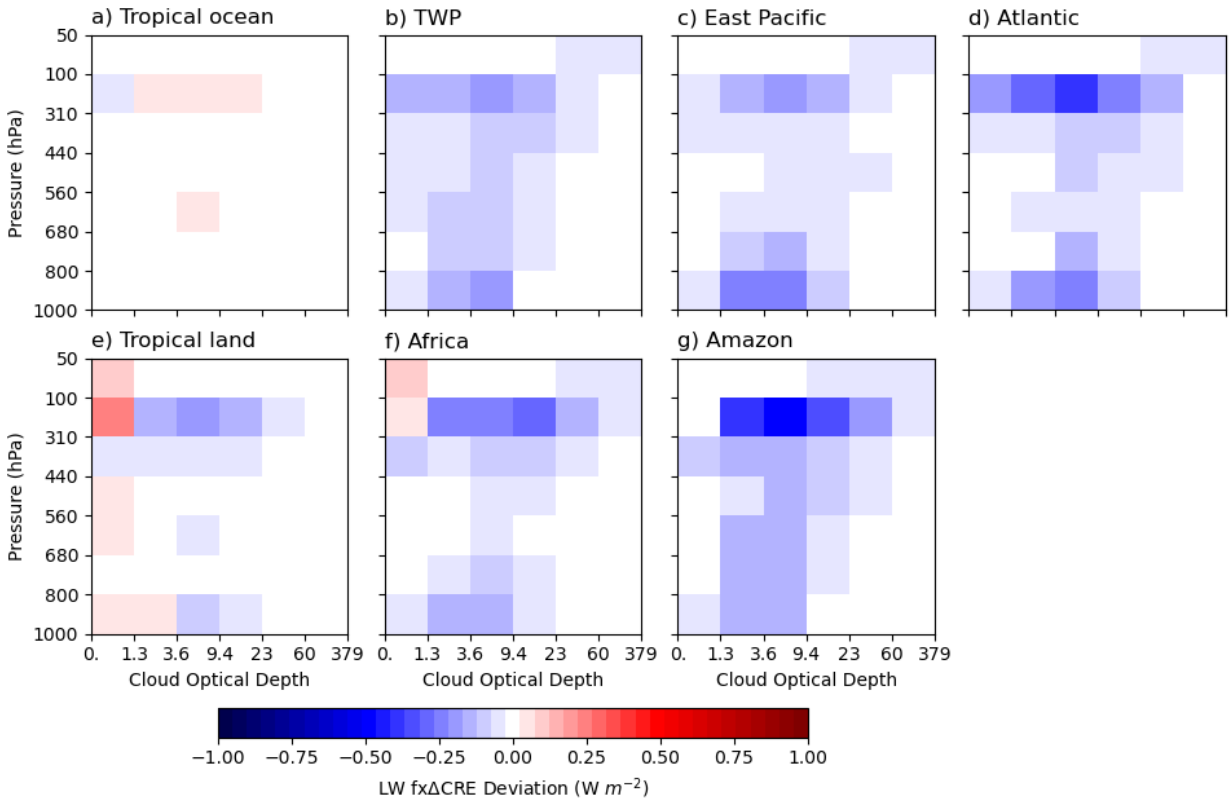

Figure 4. As in Figures 1a-g, except for the CRE deviation component of longwave CRE decomposition. Unit is W m^{-2}.

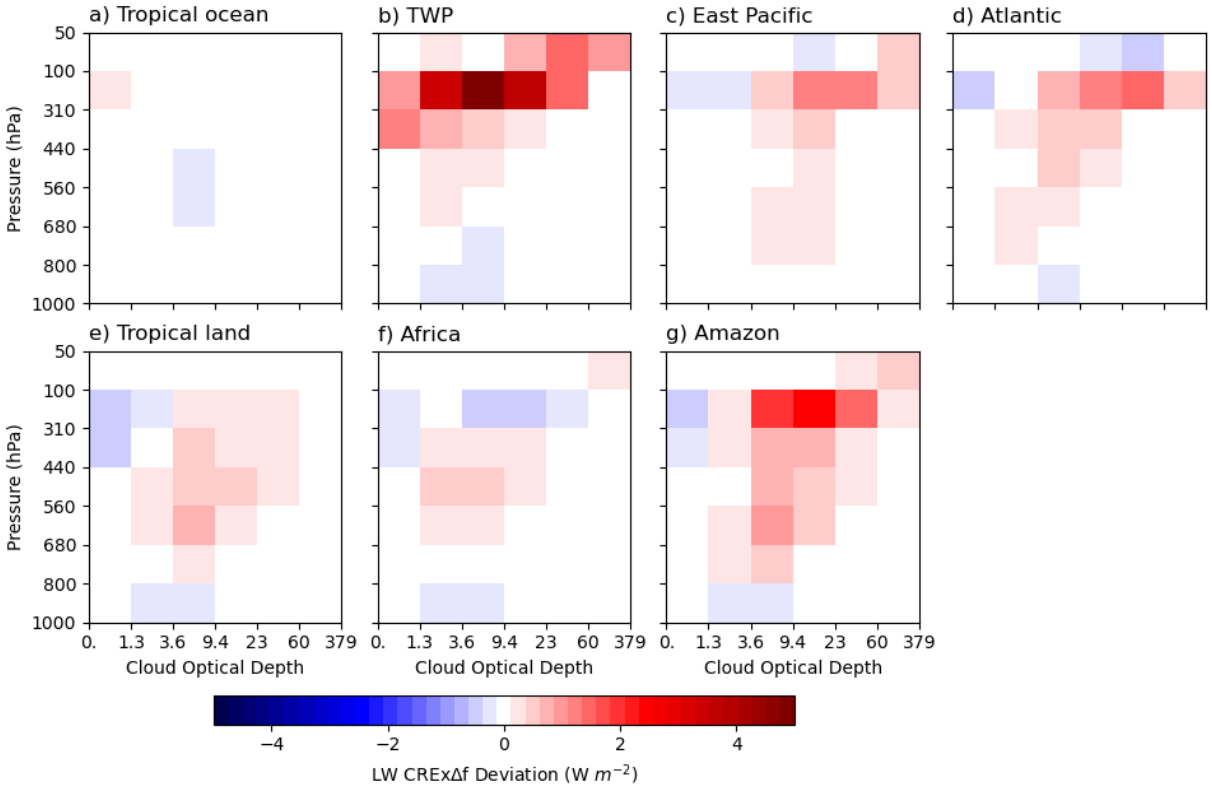

Figure 5. As in Figures 1a-g, except for the cloud fraction deviation component of longwave CRE decomposition. Unit is W m^{-2}.

827

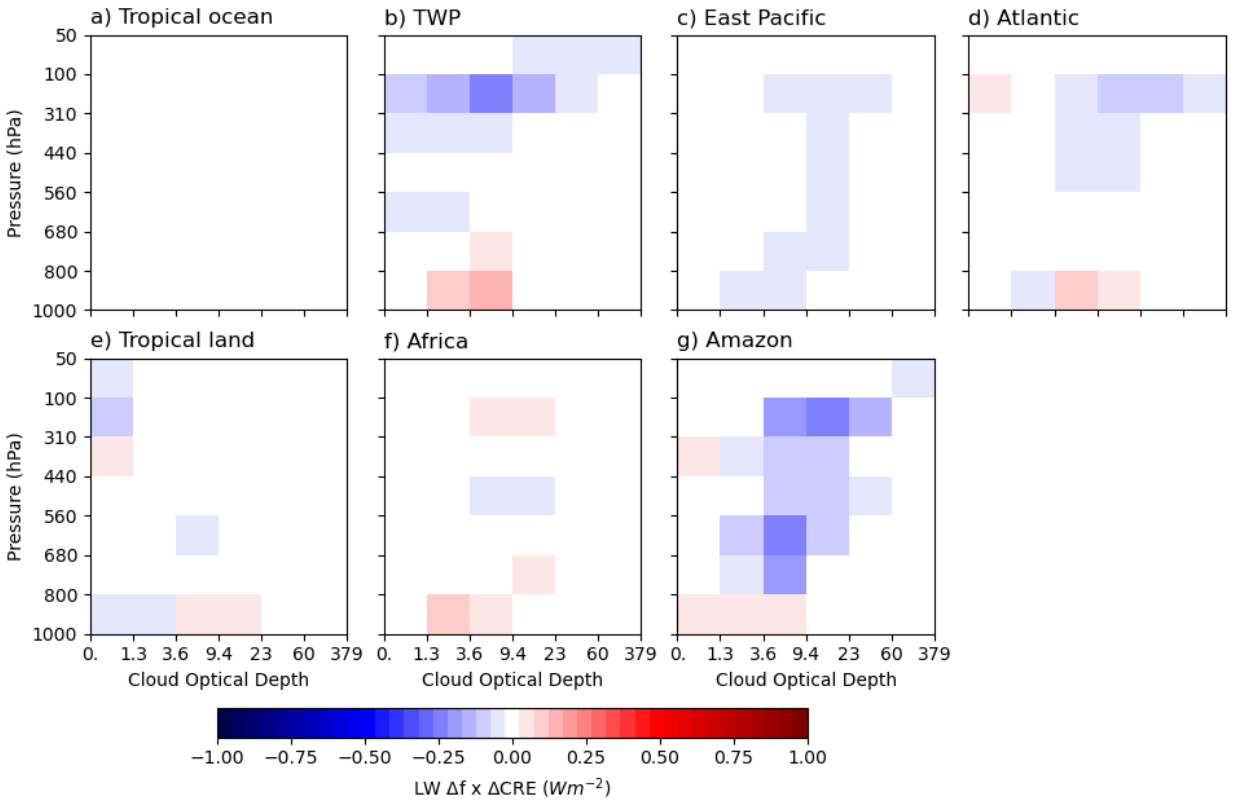

Figure 6. As in Figures 1a-g, except for the combined cloud fraction and CRE deviation component of longwave CRE decomposition. Unit is W m^{-2}.

828

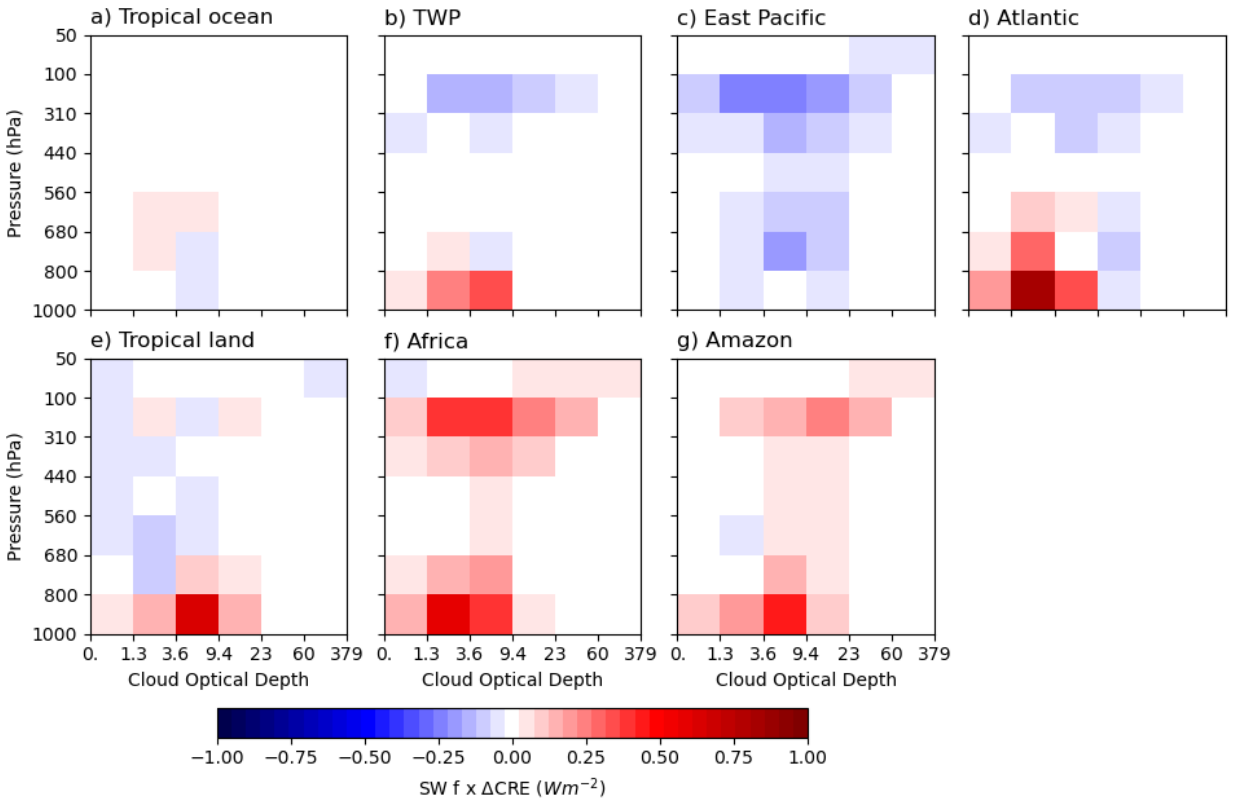

Figure 7. As in Figures 4, except for the CRE deviation component of shortwave CRE decomposition.

832

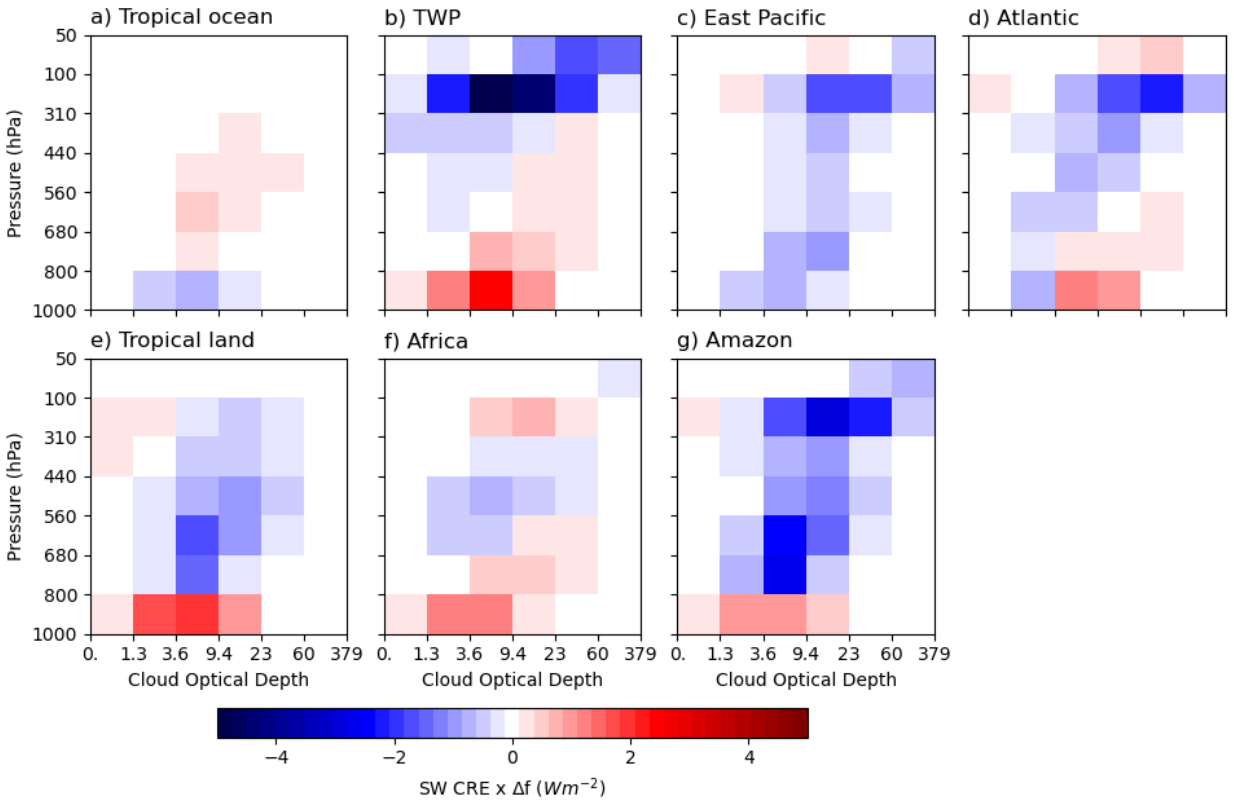

Figure 8. As in Figure 5, except for the cloud fraction deviation component of shortwave CRE decomposition.

833
834
835

836

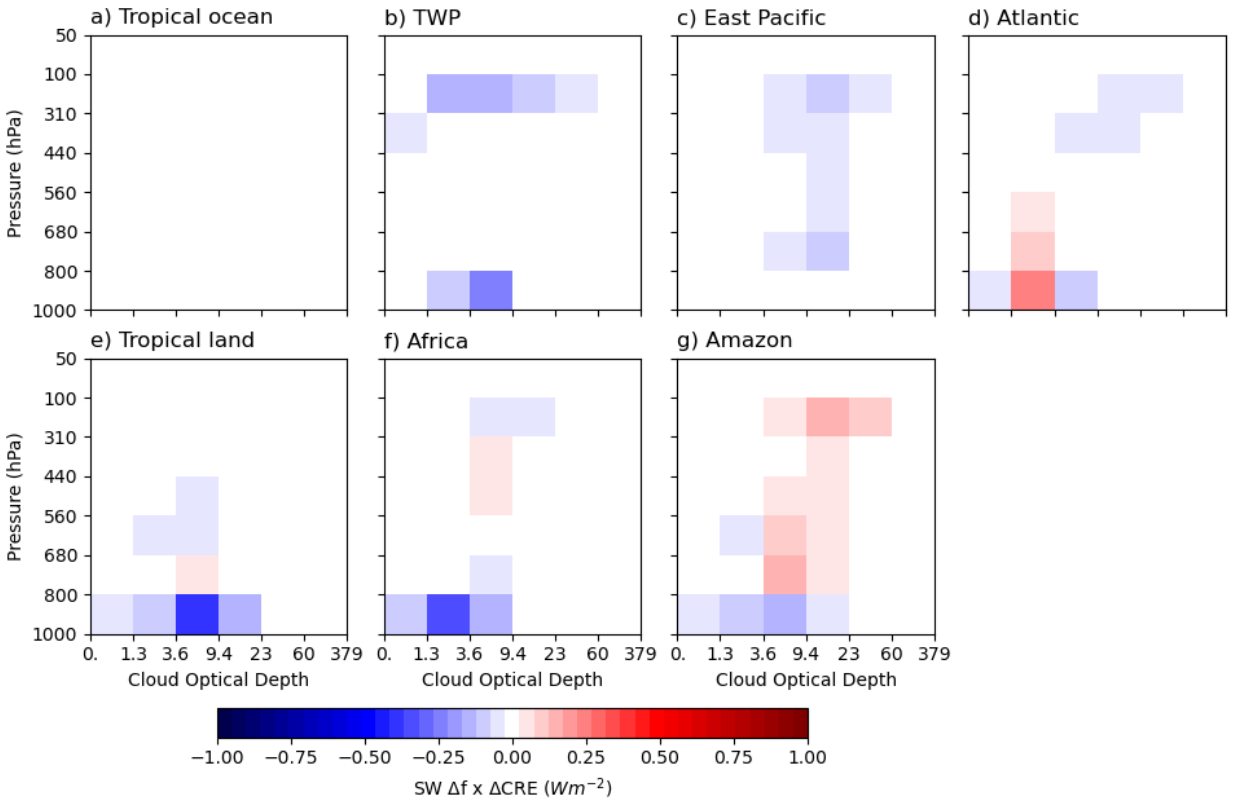

Figure 9. As in Figure 6, except for the combined cloud fraction and CRE deviation component of shortwave CRE decomposition.

837
838

839

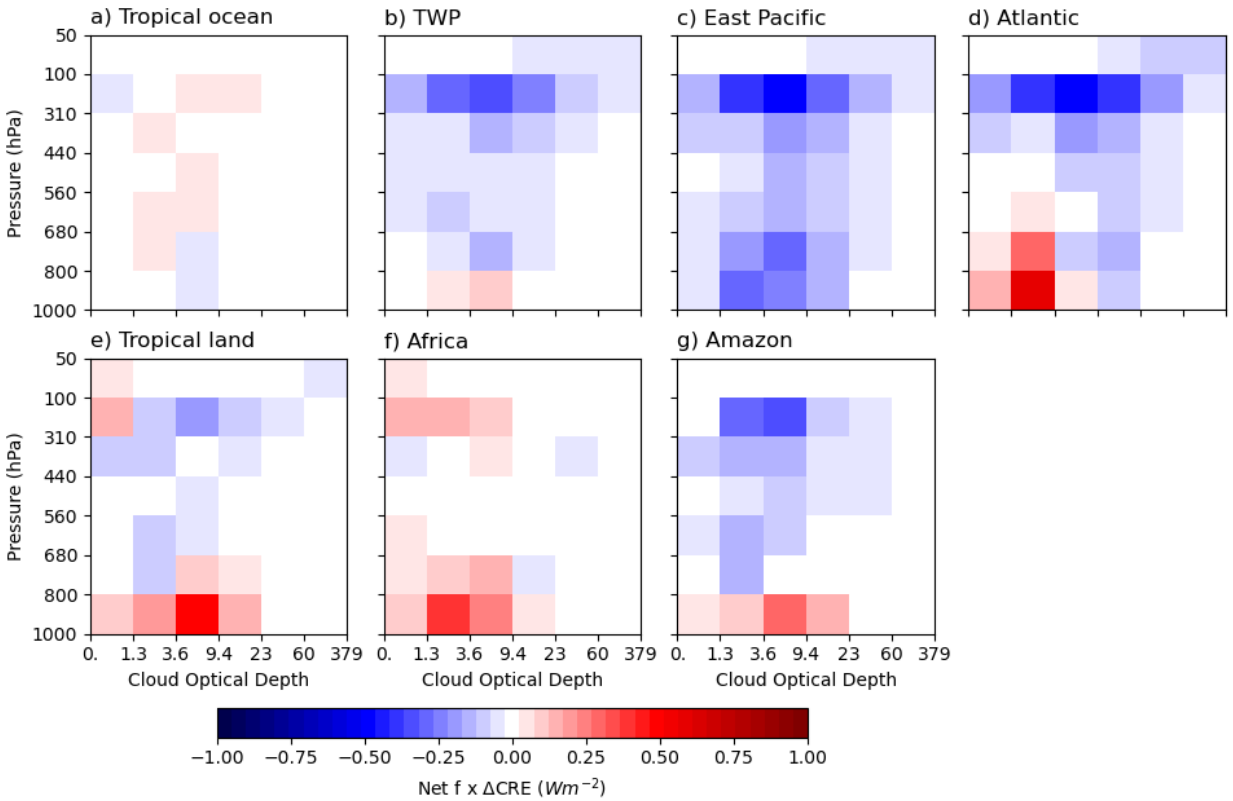

Figure 10. As in Figure 4, except for the CRE deviation component of net CRE decomposition.

840

841

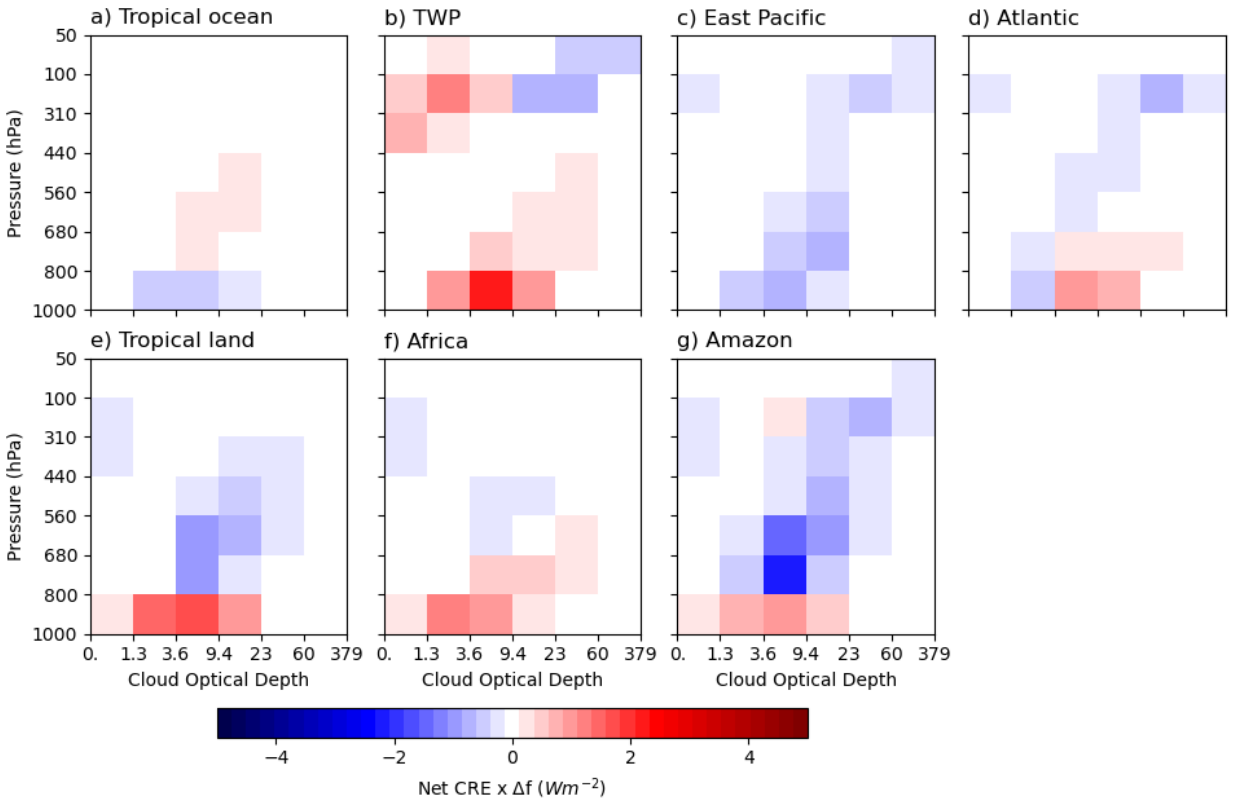

Figure 11. As in Figure 5, except for the cloud fraction deviation component of net CRE decomposition.

842
843

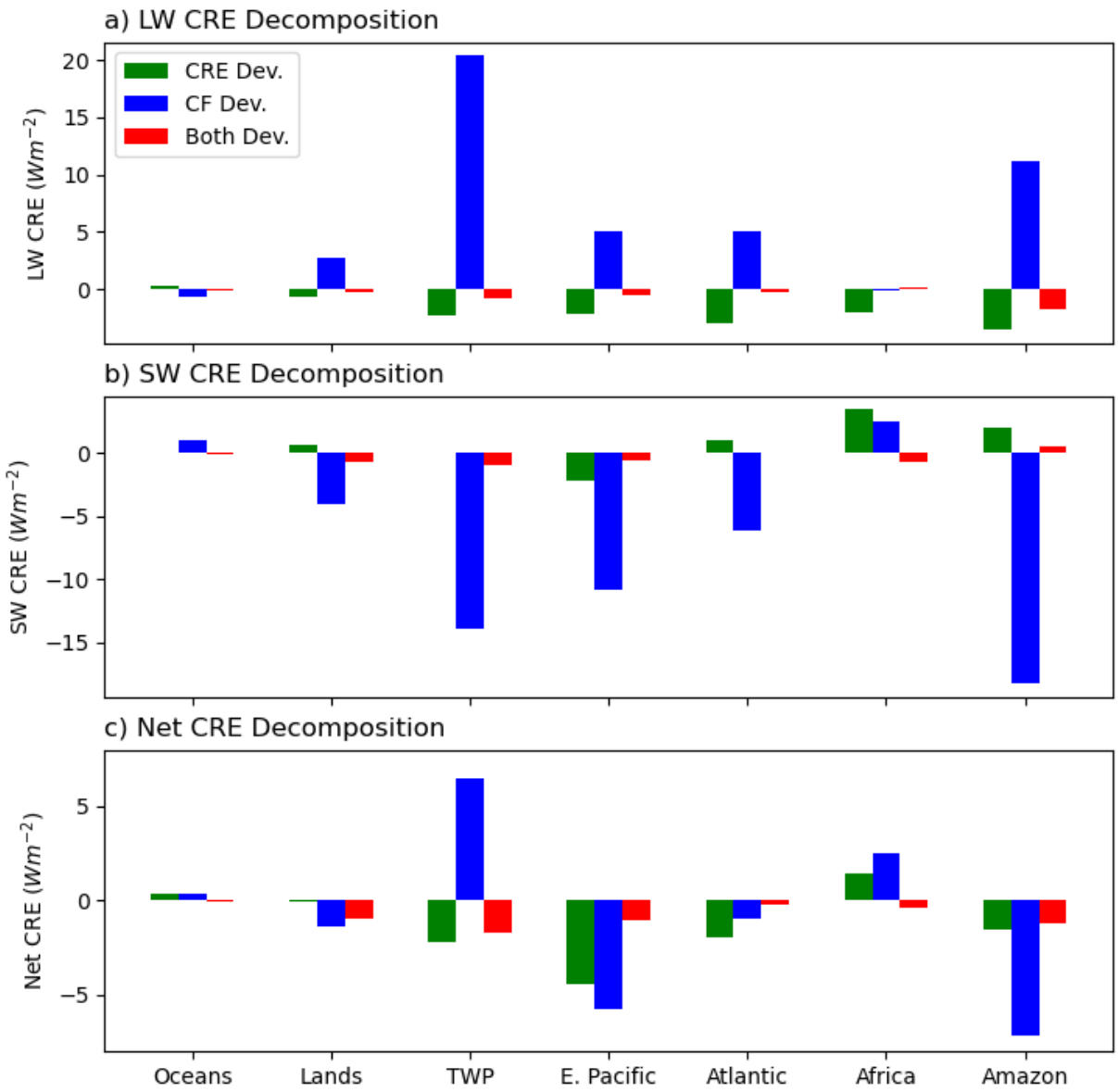

Figure 12. Differences in longwave (a), shortwave (b), and net (c) cloud radiative effects (CREs) from the tropical mean (LW: 23.4 W m^{-2}, SW: -39.6 W m^{-2} and net: -16.3 W m^{-2}), attributed to CRE deviation (green), cloud fraction (CF) deviation (blue) and the combined deviations (red), for tropical oceans, lands, the Tropical Western Pacific (TWP), East Pacific, Atlantic, Africa and the Amazon.

844